Revision 2

Trace element partitioning between olivine and melt in lunar basalts

Sha Chen[1], Peng Ni[1], Youxue Zhang[1*], and Joel Gagnon[2]

[1]Department of Earth and Environmental Sciences, University of Michigan, Ann Arbor, MI 48109, USA

[2]School of the Environment, University of Windsor, Windsor, ON, N9B 3P4, Canada

Abstract

Mineral/melt partition coefficients have been widely used to provide insights into magmatic processes. Olivine is one of the most abundant and important minerals in the lunar mantle and mare basalts. Yet, no systematic olivine/melt partitioning data are available for lunar conditions. We report trace element partition data between host mineral olivine and its melt inclusions in lunar basalts. Equilibrium is evaluated using the Fe-Mg exchange coefficient, leading to the choice of melt inclusion-host olivine pairs in lunar basalts 12040, 12009, 15016, 15647, and 74235. Partition coefficients of 21 elements (Li, Mg, Al, Ca, Ti, V, Cr, Mn, Fe, Co, Y, Zr, Nb, Gd, Tb, Dy, Ho, Er, Tm, Yb and Lu) were measured. Except for Li, V, and Cr, these elements show no significant difference in olivine-melt partitioning compared to the data for terrestrial samples. The partition coefficient of Li between olivine and melt in some lunar basalts with low Mg# (Mg# < 0.75 in olivine, or < ~0.5 in melt) is higher than published data for terrestrial

* Corresponding author. Email address: youxue@umich.edu

samples, which is attributed to the dependence of D_{Li} on Mg# and the lack of literature D_{Li} data with low Mg#. The partition coefficient of V in lunar basalts is measured to be 0.17 to 0.74, significantly higher than that in terrestrial basalts (0.003 to 0.21), which can be explained by the lower oxygen fugacity in lunar basalts. The significantly higher D_V can explain why V is less enriched in evolved lunar basalts than terrestrial basalts. The partition coefficient of Cr between olivine and basalt melt in the Moon is 0.11 to 0.62, which is lower than those in terrestrial settings by a factor of approximately 2. This is surprising because previous authors showed that Cr partition coefficient is independent of fO_2. A quasi-thermodynamically-based model is developed to correlate Cr partition coefficient to olivine and melt composition and fO_2. The lower Cr partition coefficient between olivine and basalt in the Moon can lead to more Cr enrichment in the lunar magma ocean, as well as more Cr enrichment in mantle-derived basalts in the Moon. Hence, even though Cr is typically a compatible element in terrestrial basalts, it is moderately incompatible in primitive lunar basalts, with a similar degree of incompatibility as V based on partition coefficients in this work, as also evidenced by the relatively constant V/Cr ratio of 0.039 ± 0.011 in lunar basalts. The confirmation of constant V/Cr ratio is important for constraining concentrations of Cr (slightly volatile and siderophile) and V (slightly siderophile) in the bulk silicate Moon.

Keywords: partition coefficients, lunar basalts, olivine, melt inclusions, Cr/V ratio

1. Introduction

Mineral/melt partition coefficients have been widely used to provide insights into magmatic processes. Olivine is one of the most abundant and important minerals in the lunar mantle and mare basalts. Olivine fractionation in the lunar magma ocean (LMO) and during lunar basalt differentiation plays a significant role in the evolution of the magma (Wood et al. 1970; Longhi 1977; Solomon and Longhi 1977; Snyder et al. 1992; Elardo et al. 2011; Lin et al. 2017; Charlier et al. 2018; Rapp and Draper 2018). Olivine-melt partitioning also plays a role in controlling the composition of mantle-derived basalts. Hence, quantifying olivine-melt partitioning is critical to understanding and modeling magma evolution of the LMO and lunar basalts.

Although numerous partitioning studies have been published for olivine and basaltic melt, they show significant variability for most elements due to the wide range of compositions, conditions, and methods involved. For example, the Ti partition coefficient between olivine and melt varies by more than two orders of magnitude, ranging from 0.0019 to 0.43 (Duke 1976; Rollinson 1993; McDade et al. 2003; Spandler and O'Neill 2010; Papike et al. 2013; Laubier et al. 2014; Burnham and O'Neill 2016; Leitzke et al. 2016). In addition, these studies often focus on terrestrial samples and physicochemical conditions. Though lunar and terrestrial basalts share many similarities in terms of their chemical composition, they are distinct in several aspects. Compared to typical terrestrial basalts, lunar basalts have highly variable TiO_2, lower Al_2O_3 and alkalis, and often higher FeO and Cr_2O_3 concentrations. For example, terrestrial basalts rarely contain $\geq$ 5 wt% TiO_2 in the melt due to Fe-Ti oxide saturation at ~1100 °C (Toplis and Carroll

1995), whereas lunar basalts may contain up to 14 wt% TiO_2. Such compositional differences have been shown to affect the physical properties of the melt, metal solubility in silicate melts (Borisov et al. 2004), and mineral/melt partition coefficients of multiple elements (Xirouchakis et al. 2001; Dygert et al. 2013; Leitzke et al. 2016). Another important difference between lunar and terrestrial conditions that might affect elemental partitioning behavior is the oxygen fugacity (fO_2). The fO_2 has been estimated to be approximately IW - 1 for lunar mantle and basalts (Sato et al. 1973; Wadhwa 2008), but ~ QFM for the terrestrial upper mantle (O'Neill et al. 2018), representing a difference of over four orders of magnitude. Therefore, partition coefficients for multivalent elements, such as V, Cr, Fe and Ti, could be significantly different under lunar conditions.

Chen et al. (2015) and Ni et al. (2017, 2019) have published a dataset of major element concentrations in melt inclusions and their olivine hosts, as well as trace element data in melt inclusions in a number of lunar basalts. In this study, we supplement the data of Ni et al. (2019) with trace element measurements in olivine to estimate their partition coefficients. We also examine new olivine-melt inclusion pairs in lunar basalt 12009. Here we report partition coefficients of 21 major and trace elements between olivine and melt in lunar basalts and compare the obtained partition coefficients with published data for terrestrial conditions.

2. Samples and Methods

2.1. General considerations

79 The compositions of a homogenized melt inclusion (MI) and its host olivine can be used to
80 estimate mineral/melt partition coefficients. A melt inclusion is a droplet of melt that becomes
81 trapped during mineral crystallization. At the time of entrapment, a melt inclusion can be
82 considered to be in equilibrium with the host mineral. If well preserved, coexisting host minerals
83 and melt inclusions can be analyzed to estimate partition coefficients (e.g., Nikogosian and
84 Sobolev 1997; Thomas et al. 2002; Zajacz and Halter 2007) and may have advantages over
85 experimental methods. For example, naturally-occurring, coeval host mineral/melt inclusions
86 reflect natural composition and conditions and, therefore, can more accurately represent
87 geological processes.
88 This method, however, also has its disadvantages. The compositions of melt inclusions can
89 be affected during natural cooling, including post-entrapment crystallization and diffusive
90 exchange between the melt inclusion and the host crystal as well as the magma surrounding the
91 host crystal. Post-entrapment crystallization of the host mineral into the melt inclusion as well as
92 crystallization of the melt inclusion during cooling is supposed to be reversed (corrected for) by
93 laboratory homogenization, which was carried out for all melt inclusions in this study. Whether
94 homogenization reverses post-entrapment crystallization can be evaluated by whether
95 equilibrium is reached for Fe-Mg exchange between a given melt inclusion and its host olivine.
96 Diffusive exchange occurs during cooling between melt inclusions and magma surrounding of
97 the host olivine, or between the melt inclusion and olivine. The extent of exchange depends on
98 the cooling rate, diffusivity, and compatibility of the element, size of the olivine host and melt

99 inclusion, and residence time of the host crystal in the magma. Significant diffusive exchange
100 between a melt inclusion and melt surrounding the host olivine would occur when the cooling
101 rate is 1 to 2°C/year or lower (Gaetani and Watson 2000, 2002). All lunar samples investigated
102 in this work cooled at >10°C/hour (see Section 2.2), which is 4 to 5 orders of magnitude faster
103 than 1 to 2°C/year. Furthermore, most of the samples reported here (except 12009) have been
104 examined for volatile concentrations (Ni et al. 2019), which showed, with the exception of H_2O,
105 preservation of rapidly diffusing components, such as F, Cl, and S. Such observations indicate
106 negligible diffusive exchange for the elements examined here, which, with the exception of Li,
107 diffuse more slowly than F (e.g., Zhang et al. 2010).
108 All melt inclusions studied in this work were crystalline. Naturally glassy melt inclusions
109 (such as those in 74220 studied by Hauri et al. 2013; Chen et al. 2015; Ni et al. 2019) did not
110 satisfy our selection criterion. Therefore, homogenization was needed. For homogenization
111 experiments, it is difficult to completely restore the MI composition to that at the time of
112 entrapment (i.e., equilibrium). Therefore, a criterion is needed to assess whether there is
113 approximate equilibrium between the melt inclusion and the host olivine. The Fe/Mg exchange
114 coefficient K_D (= $(FeO/MgO)_{olivine}/(FeO/MgO)_{melt}$) between olivine and basaltic melt was used to
115 evaluate whether there is approximate olivine-melt equilibrium.
116 Roeder and Emslie (1970) first showed that the Fe^{2+}-Mg exchange coefficient between
117 olivine and melt is independent of temperature and equals 0.30 ± 0.03 at equilibrium. This
118 exchange coefficient has been widely used in equilibrium calculations ever since (e.g., Langmuir

and Hanson 1980). Longhi et al. (1978), using lunar samples, reached a similar conclusion but noted decreasing K_D with increasing TiO_2. Xirouchakis et al. (2001) further studied the effect of TiO_2 concentration in melt and found that K_D can vary from 0.36 to 0.22 with a TiO_2 increase from <1 wt % to 20 wt %. From the data summarized in Xirouchakis et al. (2001), an equation showing this dependence was fitted ($K_D = -0.006668 \cdot TiO_2 + 0.35$) and used in this work. We allowed a variation of ± 0.06 (~20 % relative) in K_D from the calculated value in choosing olivine-inclusion pairs thought to be in equilibrium. Using this criterion, we have chosen previously investigated lunar samples 12040, 15016, 15647, and 74235 (Ni et al. 2019) for trace element measurement in olivine. In addition, a new lunar sample (12009) that we investigated also satisfied the criterion and was included in this study.

2.2. Sample description and preparation

Olivine-melt inclusion pairs in five lunar basalts, 12009, 12040, 15016, 15647, and 74235, satisfy the criterion for equilibrium based on the apparent K_D between the host olivine and melt inclusion, and were analyzed to obtain olivine-melt partition coefficients. Among the five lunar samples, four (all except 12009) were examined for volatiles in olivine-hosted melt inclusions by Ni et al. (2019). One sample (74235) is a high-Ti basalt, and the other four samples are low-Ti basalts. A brief description of each sample is presented here. Sample 12040 is an olivine basalt with mm-size crystals and ~ 2.6 wt% TiO_2. Accumulation of olivine was inferred for the sample (Newton et al. 1971). Sample 15016 is an olivine-normative basalt with ~2.3 wt% TiO_2 and ~50

vol.% vesicularity. Ca- or Fe-rich zonation in pyroxene indicates rapid crystallization. Sample 15647 is an olivine basalt with sub-mm size crystals and containing ~2.4 wt% TiO_2. Sample 74235 is a fine-grained high-Ti basalt (~12.3 wt% TiO_2) containing skeletal phenocrysts of olivine, pyroxene and ilmenite. Sample 12009 is a rapidly cooled low-Ti (3.3 wt% TiO_2) olivine vitrophyre basalt with large vesicles. More detailed descriptions of these samples can be found in The Lunar Sample Compendium (https://curator.jsc.nasa.gov/lunar/lsc/) and Ni et al. (2019).

Cooling rates of 74235, 12009, and 12040 have been estimated and are all greater than 10 °C/hour (Donaldson et al. 1975; Usselman et al. 1975; Walker et al. 1976). For 15016 and 15647, no cooling rate data are available. Based on the H_2O/Ce ratio versus cooling rate relation in Ni et al. (2019), they should have quenched faster than 12040, meaning a cooling rate greater than 10 °C/hour. Hence, all lunar samples we studied cooled much more rapidly than 2°C/year, with 12040 cooling the slowest, and 15647 a close second.

The radii of the investigated melt inclusions range from 13 to 22.5 μm (Table 2). Grain sizes in crystalline melt inclusions are typically small, sub-micrometers to a few micrometers for silicate minerals (Figure 1, and Newton 1971), but there might be larger metal or oxide mineral grains (brighter crystals in the lower right of Figure 1), and shrinkage bubbles.

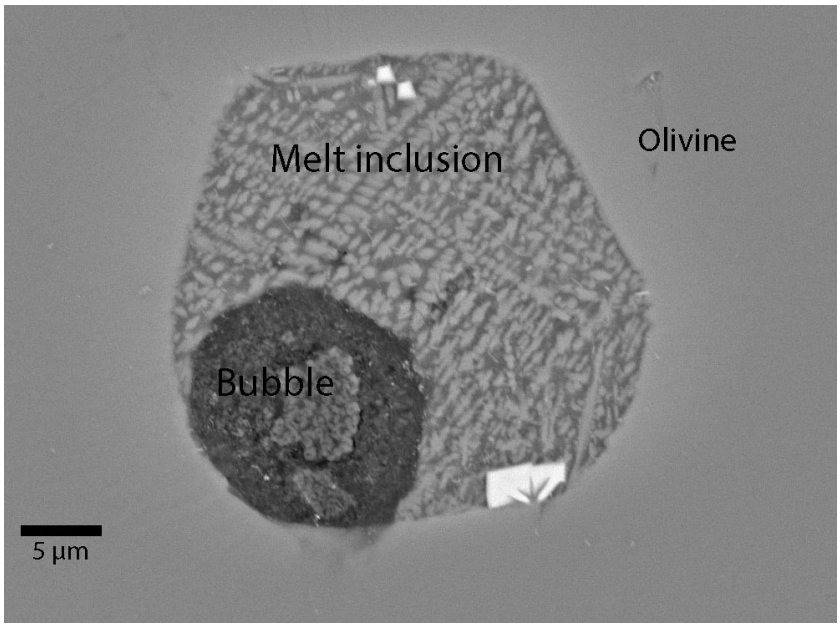

Figure 1. BSE image of a crystalline melt inclusion in olivine in lunar sample 12009 (12009-OL1-MI1) without homogenization.

155

156 Homogenization experiments were conducted at 1 bar at a temperature slightly above the
157 liquidus of the corresponding lunar rock. The olivine-hosted melt inclusions in 12040, 15016,
158 15647, and 74235 were homogenized by Ni et al. (2019), and those in sample 12009 were
159 homogenized in this study following the procedures in Chen et al. (2015) and Ni et al. (2017,
160 2019). An olivine grain from 12009 was placed in a graphite crucible (drilled from purified
161 99.995% graphite rod ordered from graphitestore.com) under continuous high purity N_2 flow to
162 maintain a reducing environment, heated to 1240 to 1250 ºC at one bar for 2 minutes, and
163 quickly quenched by immersing the crucible in water. The fO_2 in the crucible was measured to be
164 between IW-1.9 and IW-2.6 (Ni et al. 2017). The reducing condition prevented olivine oxidation,
165 but did not establish a new fO_2 for the olivine-inclusion equilibrium due to the short duration of
166 the experiments. That is, the fO_2 condition is expected to be unchanged from that during eruption

and crystallization on the Moon. More detailed description of the homogenization experiments may be found in Chen et al. (2015) and Ni et al. (2017, 2019).

The homogenized melt inclusions are essentially glassy (Figure 2) but occasionally there are undissolved metal/sulfide/oxide grains. Silicate crystals of a few micrometers in size or smaller can be dissolved in ≤ 10 s at the experimental temperatures (Chen and Zhang 2008, 2009). Diffusion distance $(Dt)^{1/2}$ (here D is diffusivity, not partition coefficient) in a MORB melt during olivine dissolution at the experimental temperature for 2 minutes is 41 μm for MgO, and 24 μm for the slower diffusing SiO_2 and Al_2O_3 using diffusivities in Chen and Zhang (2008). Diffusivities in lunar basalts are higher than those in MORB by a factor of about 4 (Morgan et al. 2006; Yu et al. 2016), meaning diffusion distances would be 2 times those in MORB, which equate to approximately 82 μm for MgO and 48 μm for SiO_2 and Al_2O_3. All melt inclusions in this study have radii smaller than 23 μm (Table 2). Hence, diffusion is able to homogenize the melt inclusions in 2 minutes except for the presence of larger grains of metal or oxide or sulfide.

After homogenization, the olivine crystals were polished to reveal the enclosed melt inclusions (Figure 2). The diameter of each melt inclusion was measured and reported in Table 2. Major and trace element concentrations in both melt inclusions and host mineral grains were analyzed.

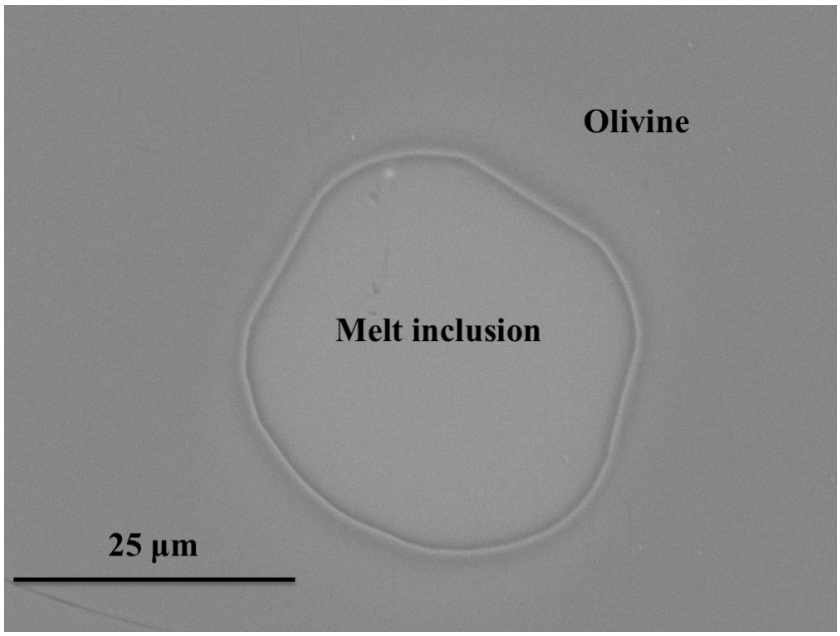

Figure 2: BSE image of a homogenized melt inclusion in olivine in 12009 (12009-OL6-MI1).

185

186

187 **2.3. Major and trace element concentration measurement**

188 **2.3.1. Major element analysis**

189 Major element concentrations of melt inclusions and host olivine grains were analyzed using
190 a CAMECA SX-100 electron microprobe (EMPA) at the University of Michigan. Analyses were
191 carried out using a 15 kV, 10 nA, and 5 µm defocused beam in wavelength-dispersive
192 spectrometry (WDS) mode. At least five points were measured on the host olivine at locations
193 adjacent to each melt inclusion. Fewer data points were obtained for some melt inclusions due to
194 the limitation of their small sizes. Data are reported in Table 1 (all tables are in an Excel file for
195 easy use by readers). We only report olivine-melt inclusion pairs that were considered to be
196 approximately in equilibrium based on their apparent Fe^{2+}-Mg K_D values.

197

198 **2.3.2. Trace element concentrations in melt inclusions**

199 Trace element concentrations in melt inclusions were analyzed using secondary ion mass
200 spectrometry (SIMS) at California Institute of Technology using a Cameca IMS 7f- GEO. Trace
201 element measurements for sample 12009 were conducted in this study, while those for lunar
202 samples 12040, 15016, 15647, and 74235 are from Ni et al. (2019). The analytical procedures are
203 very similar and briefly described below.

204 Twenty-two trace elements (Li, Na, K, Sr, Y, Zr, Nb, Ba, La, Ce, Pr, Nd, Sm, Eu, Gd, Tb,
205 Dy, Ho, Er, Tm, Yb, Lu) and four transition metal elements (V, Cr, Mn, Co) were analyzed in
206 two separate sessions. For the analyses of trace elements, a 10 to 13 nA O^- primary ion beam was
207 used to generate secondary ion signals for measurement. Sensitivity factors were calculated
208 using the internal standard of ^{30}Si based on reported concentrations in NIST glass standard SRM
209 610 (Pearce et al. 1997). Accuracy of the analyses was verified by measuring two additional
210 NIST standards (NIST 612 and NIST 614) and two MPI-DING glass standards (GOR128-G and
211 KL2-G). For the analyses of transition metal elements, an 11 to 17 nA O^- primary ion beam was
212 used and a mass resolution power (MRP) of 5500 was applied to the mass spectrometer to
213 separate interferences from the target masses.

214 Most data on olivine-hosted melt inclusions are from Ni et al. (2019), and the calibration
215 curves are shown and discussed there. Calibration curves for the transition metal elements for
216 12009 can be found in Supplementary Figure S5. Calculated concentrations in standards in this
217 work are compared with reference values (Jochum et al., 2005, 2006, 2011) in Figure S6 and

Table S2. Nickel concentrations were also measured, but the measured concentrations in some standards can differ from reference values by more than a factor of 4. Hence, Ni data are not used.

2.3.3. Trace element concentrations in olivine

Trace element analyses for all olivine crystals reported in this study were carried out using a laser ablation inductively coupled plasma mass spectrometry (LA-ICP-MS) system in the Element and Heavy Isotope Analytical Laboratories at the University of Windsor. The instrumentation comprises a Photon Machines Analyte Excite 193 nm, short (sub 4 ns) pulse width Ar-F Excimer laser ablation system coupled with an Agilent 7900, fast scanning quadrupole ICP-MS. For each LA-ICP-MS analysis, 30 s of gas and instrument background were acquired with the laser off, followed by 40 s ablation signal with the laser on. The laser was operated at a pulse energy of 120 mJ and a repetition rate of 5 Hz, with 60 % output power. Three spot sizes, 50 μm, 85 μm, and 110 μm, were applied depending on olivine crystal size.

Most trace elements are highly incompatible in olivine relative to the coexisting silicate melt, thus leading to their extremely low concentrations. The concentrations of Na, K, La, Ce, Pr, Nd, Sm, Eu, Nb, Mo, and Sn in olivine were found to be below detection limit. Nonetheless, eighteen trace elements (using isotopes of ^{7}Li, ^{27}Al, ^{49}Ti, ^{51}V, ^{52}Cr, ^{55}Mn, ^{59}Co, ^{89}Y, ^{90}Zr, ^{93}Nb, ^{157}Gd, ^{159}Tb, ^{163}Dy, ^{165}Ho, ^{166}Er, ^{169}Tm, ^{172}Yb and ^{175}Lu) were successfully measured and their concentrations with 1σ errors are reported in Table 2. When possible, two isotopes per element

(^{6}Li and ^{7}Li, ^{47}Ti and ^{49}Ti, ^{52}Cr and ^{53}Cr, ^{60}Ni and ^{62}Ni, ^{66}Zn and ^{68}Zn, ^{90}Zr and ^{91}Zr, ^{95}Mo and ^{98}Mo, ^{116}Sn, ^{118}Sn, and ^{119}Sn) were measured to check for reproducibility and mass interferences.

NIST standards 610, 612, 614, and 616 plus three MPI-DING standards (GOR128-G, GOR132-G, St-Hs-G) were used as external calibration standards. The NIST standards are soda lime silicate glasses doped with various concentration levels of trace elements. NIST 610, 612, 614 and 616 are nominally doped with approximately 500, 50, 1 and 0.02 ppm, respectively, of most trace elements. Since all the aforementioned standards contain more than 1 wt% Al, a SRM 1830 glass with a low Al concentration (635 ppm, certified), similar to the olivine samples, was used for LA-ICP-MS calibration. ^{29}Si was used as the internal calibration standard to correct for differences in the rate of ablation between the standards and olivine crystals.

Inclusions were avoided during LA-ICP-MS measurements both by positioning the laser spot away from visible inclusions, and by assessing each spectrum for evidence of compositional change in olivine. Calibration curves are shown in Supplementary Figures S1, S2, and S3 for beam diameters of 65 μm, 85 μm, and 110 μm, respectively. When there is significant scatter in the calibration curve for a given element (e.g., Ge, Zn and Sc in Figure S1), the calibration is deemed unacceptable and elemental concentrations in samples are not calculated. The concentrations in the standards obtained in this study are compared with reference values (GeoRem, Jochum et al. 2005, 2006, 2011) in Figure S4 and Table S2.

3. Results

3.1. Comparison of melt inclusion and whole rock composition

Melt inclusions in olivine crystals studied here have a range of SiO_2 concentrations from 38.0 to 48.3 wt% and the Mg# range of the host olivine is 0.45 to 0.74. Three samples (15016, 74235, and 12009) have olivine Mg# (or Fo#) greater than 0.70, while samples 12040 and 15647 with slower cooling rate have low olivine Mg# ranging from 0.45 to 0.57.

Major oxide concentrations in melt inclusions for 74235, 15016, and 12009 are generally consistent with the whole rock. On the other hand, melt inclusions in 12040 are considerably different in composition from the whole rock, especially in MgO (4 to 6 wt% in MIs vs. ~16 wt% in whole rock, The Lunar Sample Compendium), which is consistent with accumulation of olivine in the whole rock of 12040 (e.g., Newton et al. 1971). The high FeO in olivine (36.7 and 44.4 wt%) indicates late crystallization or re-equilibration during the relatively slow cooling process (The Lunar Sample Compendium).

Another slowly cooled basalt, 15647, also contains high FeO (43.9 wt%) in olivine. The melt inclusion investigated here is enriched in FeO by ~10 wt% and depleted in MgO by ~5 wt% and SiO_2 by ~3 wt% compared with the whole rock. The high FeO concentrations in both the olivine host and the melt inclusion in sample 15647 indicate a more evolved composition than the whole rock.

3.2. Partition coefficients between olivine and melt

277 Partition coefficients and associated errors (1σ) between olivine and lunar basalt are
278 reported in Table 3. Errors are calculated using the equation: $\sigma_D = D * \sqrt{(\frac{\sigma_X}{X})^2 + (\frac{\sigma_Y}{Y})^2}$ (X and
279 Y are the concentrations in the mineral and melt inclusion, respectively). In general, Mg and Co
280 behave compatibly in olivine. Fe, Mn, and Li exhibit close to neutral compatibility. V and Cr are
281 moderately incompatible in olivine, while most other elements (Al, Ca, Ti, Y, Zr, Nb, and REEs)
282 are highly incompatible.
283 To examine whether the variation of partition coefficients is mainly due to data scatter, such
284 as measurement uncertainty or disequilibrium, partition coefficients of different elements are
285 plotted versus each other, and good correlations are found between element pairs such as REE-Y,
286 Y-Ti, Ca-Ti, Cr-Ca, and Li-Al (Figure 3). As a dominant major element in olivine, the Mg
287 partition coefficient has a narrow range (4.12 to 5.45). Hence, no obvious correlation was found
288 between D_{Mg} and the partition coefficients of any other element. There is excellent correlation
289 among REE and Y partition coefficients (Figure 3a). Furthermore, the partition coefficients of
290 REE increase with D_{Ca} and D_{Ti} (Figures 3b and 3c), and the partition coefficients of V and Cr
291 decrease with increasing D_{Ca} and D_{Ti} (Figures 3d and 3e). The partition coefficient of Al is
292 negatively correlated with that of Li (Figure 3f).
293

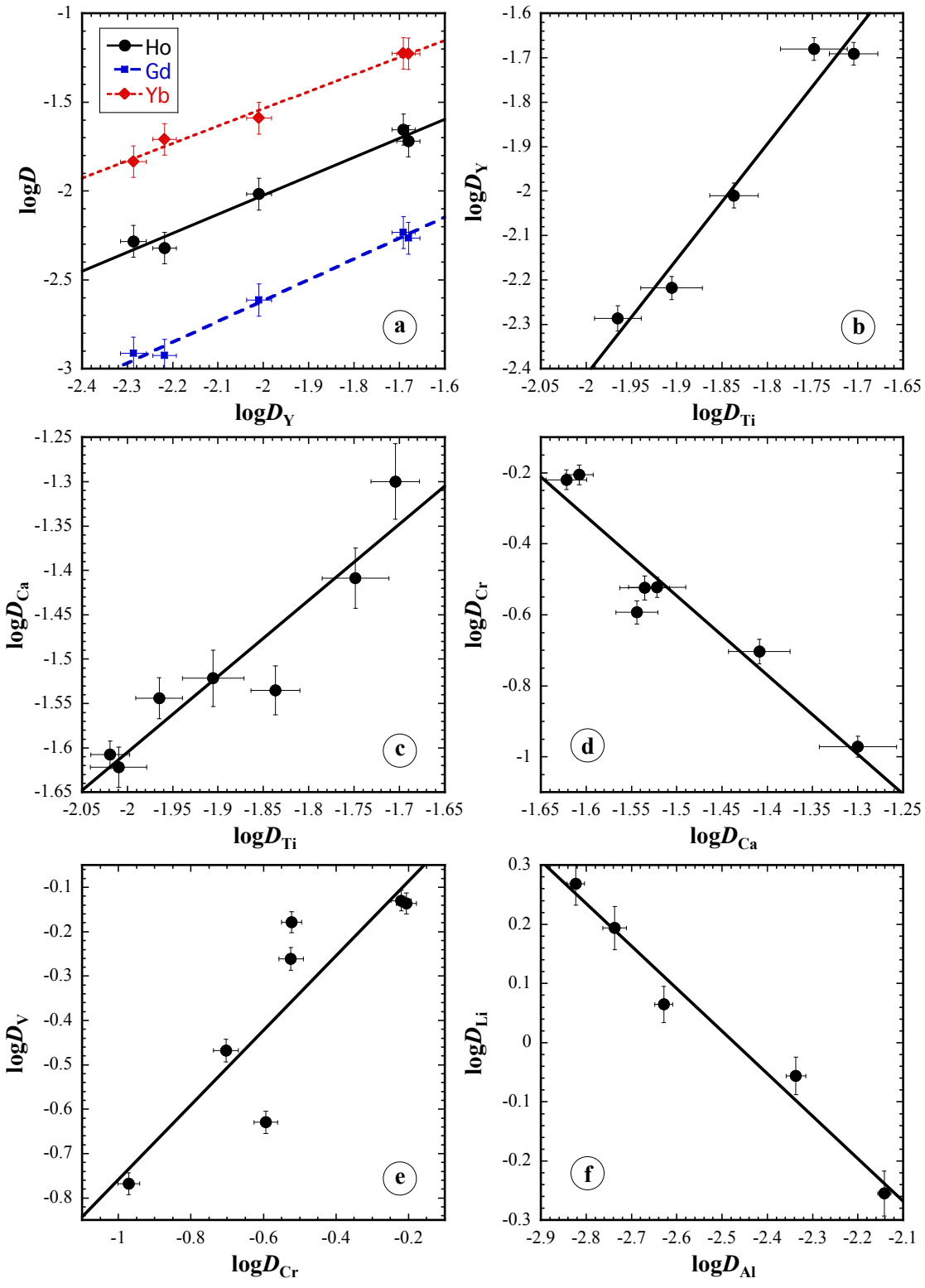

Figure 3: Correlations between partition coefficients of selected elements between olivine and melt in lunar basalts. Data are from this study. Error bars are at 1σ level.

297

298 The correlations in Figure 3 indicate that at least for the elements shown, the variation of
299 the partition coefficients is not due to measurement uncertainty or disequilibrium. Specifically,
300 the good correlation between D_{Li} and D_{Al} indicates that D_{Li} is not significantly affected by
301 disequilibrium due to post-entrapment diffusion. The most likely cause for the variation is
302 compositional dependence. Hence, we examined the dependence of the partition coefficients on
303 melt composition by plotting D versus various oxide concentrations in the melt. The dependence
304 of partition coefficients on TiO_2 in the melt is not obvious, partially because there is only one
305 high-Ti basalt in our study. Some consistent trends between the partition coefficients and oxide
306 concentrations were observed and are shown in Figure 4. For example, D_{Ca} and D_{Ti} increase with
307 FeO content of the melt (Figures 4a and 4b), whereas D_V and D_{Cr} decrease with FeO content of
308 the melt (Figures 4c and 4d). Because oxide concentrations in the limited number of melt
309 inclusions investigated in this work are not independent of each other, it is not possible to assess
310 whether or not the partition coefficients depend only on FeO. For example, D_{Ca} appears to also
311 decrease with CaO or Al_2O_3 concentration in the melt (Figures 4e and 4f), which might be an
312 artifact due to the correlation between CaO and FeO and between Al_2O_3 and FeO in the melt.
313

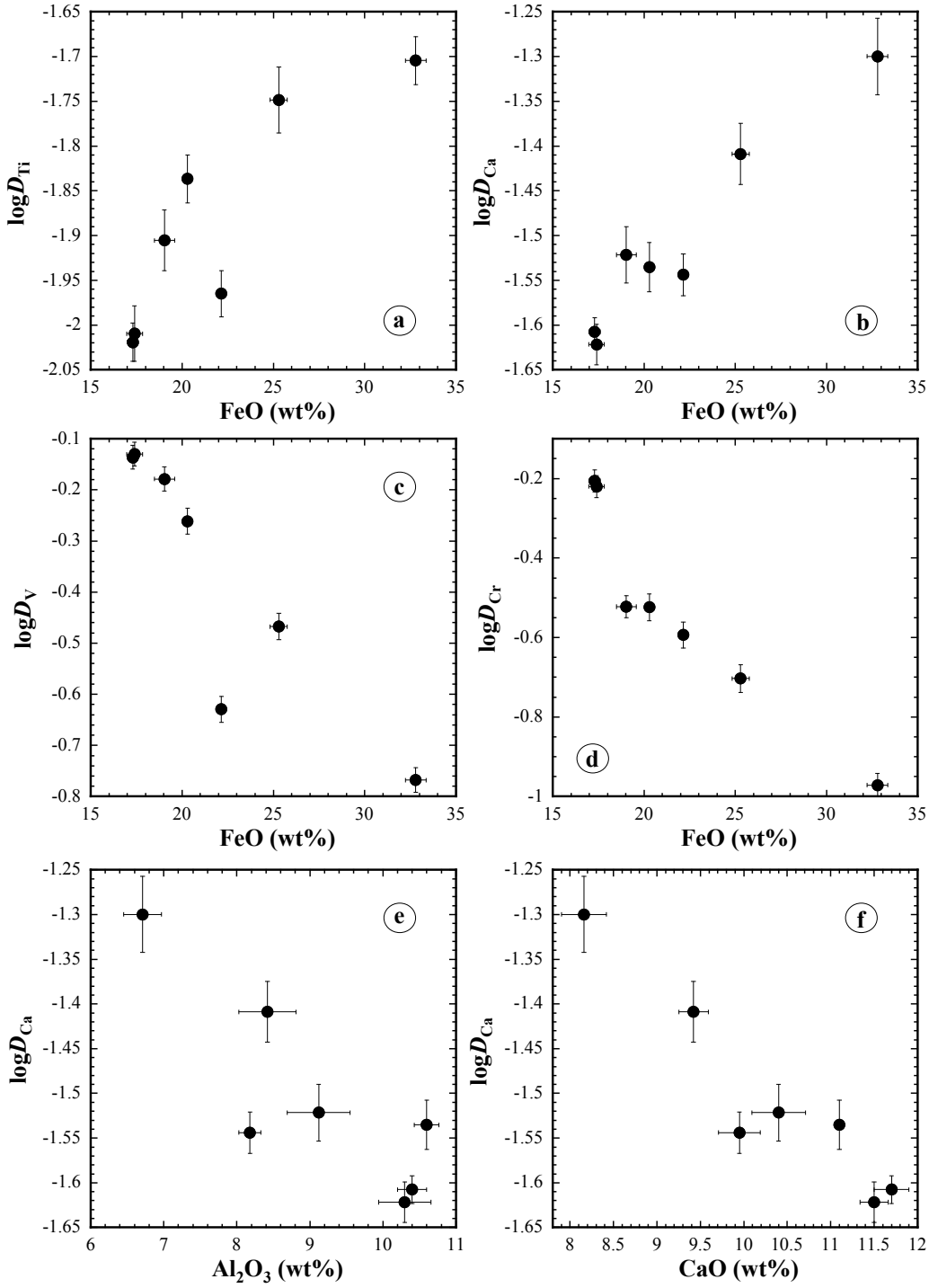

Figure 4: Dependence of partition coefficient on major oxide composition in the melt. Black dots are partition data between olivine and melt in lunar basalt from this study. Error bars are at 1σ level.

4. Discussion

4.1. Comparison with literature data

All elemental partition coefficients between olivine and melt obtained for lunar basalts in this study are shown in Table 3, together with minimum and maximum values of partition coefficients for terrestrial basalts. Figure 5 compares partition coefficients in lunar basalts (points with colored symbols) with literature data for terrestrial conditions (gray bars). The literature data for partition coefficients of each element between olivine and mafic melt typically span a large range, 0.7 to 2 orders of magnitude. For most elements, partition coefficients between lunar olivine and basalt determined in this study fall within the range of terrestrial values reported in literature. However, the partition coefficients of Li, V, Cr, Co, Dy, and Tm show differences between our data for lunar basalts and literature data for terrestrial conditions (Figure 5). The difference in D_{Dy} and D_{Tm} between lunar and terrestrial basalts is likely due to the lack of experimental data: only one paper reported experimental Dy and Tm partition data for terrestrial conditions. For example, if interpolated D_{Dy} and D_{Tm} in Nielsen et al. (1992) (as listed in Geochemical Earth Reference Model website, https://earthref.org/KDD/) were included, the terrestrial range would cover all the lunar Dy and Tm data. For Co, one lunar sample (15647) has a lower Co partition coefficient than in other lunar samples and in literature terrestrial data. The calibration curve for Co in olivine has more scatter than for other elements (Zn, Cu, and Ni calibration curves show even more scatter, and are deemed unsatisfactory and were not used).

Hence, we will not emphasize the single point. Below, we examine the differences in D_{Li}, D_{Cr} and D_V between lunar and terrestrial basalts.

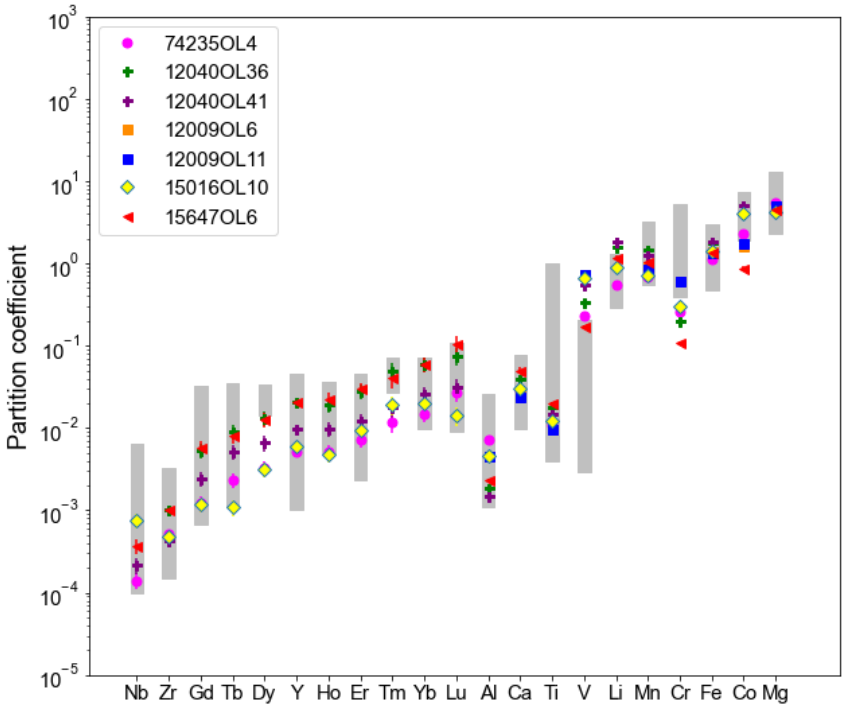

Figure 5: Partition coefficients between olivine and melt in lunar basalt from this study (colored symbols) compared with literature data at terrestrial conditions (gray vertical bars). Data and references can be found in Table 3. The partition coefficients for terrestrial basalts are selected from literature data based on the following criteria: experimental data only, logfO_2 greater than QFM-2, and melt compositions with 2 to 20 wt% FeO_t, >10 wt% Al_2O_3, and < 5 wt% TiO_2.

The partition coefficient of Li between olivine and basalt is higher in some lunar samples than in terrestrial samples. D_{Li} appears to increase with the Fa# (= Fe/(Fe+Mg) of olivine) (Figure 6a). Literature D_{Li} data are limited (Dunn and Sen 1994; Brenan et al. 1998; Taura et al. 1998; McDade et al. 2003; Ottolini et al. 2009; Dalou et al. 2012; Nielsen and Ustunisik 2019). Only 25 data points satisfy the following conditions: nominally dry, < 20% relative error on Li concentrations, containing > 30 wt% SiO_2, and having both olivine and melt composition reported. All these literature data are for low-Fa# olivine (Fa# ≤ 0.22 or Fo# ≥ 0.78), whereas D_{Li} in this work are for samples with Fa# as high as 0.55, leading to higher D_{Li} values in the Fe-rich

samples (Figure 6a). One explanation for the increase of D_{Li} with Fa# is that the ionic radius of Li^+ (0.76 Å in octahedral site, Shannon 1976) is more similar to that of high-spin Fe^{2+} (0.78 Å) than to Mg^{2+} (0.72 Å). We modeled the dependence of D_{Li} on temperature, pressure, and composition and determined that the pressure effect is insignificant. A rough fit is as follows:

$$\ln D_{Li} = 3.33 + [-13457 + 8216\sqrt{Fa\#} + 51.9(SiO_2+2Al_2O_3)]/T, \quad (1)$$

where T is in kelvin, and SiO_2 and Al_2O_3 are in wt% in the melt (i.e., 50 wt% SiO_2 means SiO_2 = 50 in the above equation, not 0.5). The above equation can reproduce $\ln D_{Li}$ data with a standard deviation of 0.19 after excluding two outlier points (Figure 6b). Based on the above equation, D_{Li} between olivine and melt increases with Fa# in olivine and SiO_2+2Al_2O_3 in the melt.

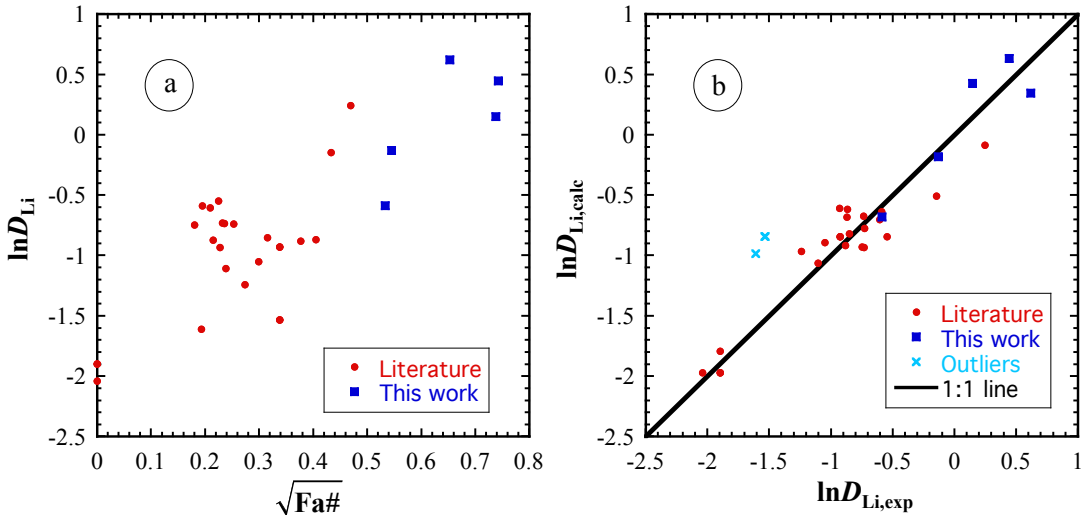

Figure 6. (a) Correlation between $\ln D_{Li}$ and square root of Fa# in olivine. (b) Comparison of calculated $\ln D_{Li}$ using Equation (1) (vertical axis) with experimental values (horizontal axis). Data sources include: Dunn and Sen 1994; Brenan et al. 1998; Taura et al. 1998; McDade et al. 2003; Ottolini et al. 2009; Dalou et al. 2012; Nielsen and Ustunisik 2019. Data with >20% relative error in Li concentration or with less than 10 wt% SiO_2 are excluded. Two outlier points are from Taura et al. (1998) and Dalou et al. (2012).

364

365 Chromium exists mainly in the form of Cr^{3+} in terrestrial basalts, but a significant fraction
366 of Cr is Cr^{2+} under the reducing conditions in lunar glass and minerals (Schreiber and Haskin
367 1976; Sutton et al. 1993; Papike et al. 2005; Berry et al. 2006; Bell et al. 2014; Simon and Sutton
368 2017). Considerable research has been devoted to Cr partitioning under terrestrial and lunar
369 conditions, showing complicated Cr partitioning behavior between olivine and melt. Schreiber
370 and Haskin (1976) determined Cr partition coefficients in forsterite-anorthite-diopside and
371 forsterite-anorthite-silica systems with an fO_2 range of about 10 orders of magnitude, and showed
372 that D_{Cr} between forsterite and melt depends on temperature, composition, and fO_2. D_{Cr} data by
373 Milkouchi et al. (1994) and Gaetani and Grove (1996) in FeO-bearing systems and a narrower
374 fO_2 range showed no dependence on fO_2. Hanson and Jones (1998) reconciled these results by
375 proposing that Cr^{3+} partitioning was sensitive to composition, whereas Cr^{2+} partitioning was
376 highly sensitive to temperature. Consequently, for a certain composition and temperature, the
377 Cr^{3+} partition coefficient is similar to that of Cr^{2+}, leading to approximately constant D_{Cr} with fO_2.
378 Mallmann and O'Neill (2009) reported that for some melts that contain < 1.7 wt% FeO at
379 1300°C, the Cr partition coefficient between olivine and melt is roughly constant between
380 QFM-10 and QFM+4. Yet, our data show that the Cr partition coefficient between olivine and
381 melt in lunar basalts is significantly lower than that in terrestrial rocks. The significantly lower
382 D_{Cr} in lunar basalts than in terrestrial basalts must be due to differences in some combination of
383 composition, fO_2, and temperature (Hanson and Jones 1998).

384 We modeled D_{Cr} as a function of temperature, olivine and melt composition, and fO_2. The
385 following criteria were used in filtering literature D_{Cr} data: 1) fO_2 values must be reported for
386 each D_{Cr} value, 2) if Cr_2O_3 concentration is measured by electron microprobe, the Cr_2O_3
387 concentration must be > 0.10 wt% so that it does not have too large an uncertainty, 3) the 1σ
388 uncertainty must be < 20% of the measured concentration, and 4) the chemical composition must
389 contain < 5 wt% other oxides in addition to the typical major oxides. Data sources are listed in
390 Figure 7.
391 We first tried using an empirical linear model in which $\ln D_{Cr}$ is assumed to be linearly
392 dependent on $1000/T$, P, $\log fO_2$, $(1\text{-Fo}\#_{oliv})^2/T$, X_i/T (where X_i is the cation mole fraction of Si, Ti,
393 Al, etc.), plus various multiplications of these terms. The model is similar to but includes more
394 complicated terms than the model of Mallmann and O'Neill (2013) for V partitioning.
395 Unfortunately, this effort did not lead to satisfactory fits (e.g., mean error in reproducing $\ln D_{Cr}$
396 being ≤ 0.2) even with ≥ 14 parameters unless some coefficients were large positive and negative
397 values, leading to wide swings in the calculated $\ln D_{Cr}$, which are indicative of overfitting.
398 We then tried to model D_{Cr} as a function of temperature, pressure, melt composition and fO_2
399 using a quasi-thermodynamically based formulation. In this formulation, D_{Cr} is related to D_{CrO},
400 $D_{CrO_{1.5}}$ (CrO_3 is not included for simplicity), and the equilibrium constant K_{hom} for the
401 homogeneous reaction of CrO(melt) $+(1/4)O_2 \rightleftharpoons CrO_{1.5}$(melt) as follows (e.g., Mallmann and
402 O'Neill, 2009):

$$\ln D_{Cr} = \ln \frac{D_{CrO} + D_{CrO_{1.5}} K_{hom} f_{O_2}^{1/4}}{1 + K_{hom} f_{O_2}^{1/4}}. \quad (2)$$

Each of $\ln D_{CrO}$, $\ln D_{CrO_{1.5}}$, and $\ln K_{hom}$ is expressed as a linear function of $1/T$, P/T, Fo#/T, X_i/T in the melt, and X_iX_j/T (e.g., regular solution model would have X_iX_j/T terms in the activity coefficients). Such a model requires nonlinear minimization involving numerous terms, which was performed using MatLab. The terms are added or removed based on the examination of fitting results. However, by increasing the number of fitting parameters to improve fitting precision, some fitting parameters would assume large positive and negative values, leading to wide swings in the calculated D_{Cr} values. After much effort, we decided to adopt the following less complicated model to avoid overfitting:

$$\ln D_{CrO} = -2.92 + 41698 \cdot Si \cdot Mg/T, \quad (3a)$$

$$\ln D_{CrO_{1.5}} = -4.52 + [5395 + 1338Fo\# + 35299Mg(Na+K)]/T, \quad (3b)$$

$$\ln K_{hom} = -79.00 + [104330 + 126061(Mg+Ca+Na+K)]/T, \quad (3c)$$

where T is temperature in kelvin, Si, Mg, Ca, Na, and K are cation mole fractions of the melt, and Fo# = Mg/(Mg+Fe) in olivine.

Using D_{CrO}, $D_{CrO_{1.5}}$, and K_{hom} in Equations (3a), (3b), and (3c) to calculate $\ln D_{Cr}$ in Equation (2), experimental $\ln D_{Cr}$ values can be reproduced with a standard deviation of 0.20 ln$D$ units (Figure 7) after excluding 15 points. However, K_{hom} values based on the fitting results parameters vary by 11 orders of magnitude over the temperature and composition range of the literature data, which may be unrealistic. Hence, even though $\ln D_{Cr}$ values can be roughly

reproduced using the fit, the physical interpretation of the fitted D_{CrO}, $D_{CrO_{1.5}}$, and especially K_{hom} may not be meaningful. Based on Equations (3a) to (3c), the lower D_{Cr} values between olivine and melt in lunar basalts may be attributed to lower Fo#, lower Si·Mg, and lower Mg(Na+K) than terrestrial basalts. Hence, key experimental data to improve understanding and modeling of Cr partition between olivine and melt appear to be those with lower Fo# (down to at least 0.5, which also means low MgO concentration in the melt) and at a large range of fO_2.

In addition to the above quasi-thermodynamically-based modeling, we also examined different substitution mechanisms to explain the variation of Cr partition coefficient, but did not arrive at satisfactory answers.

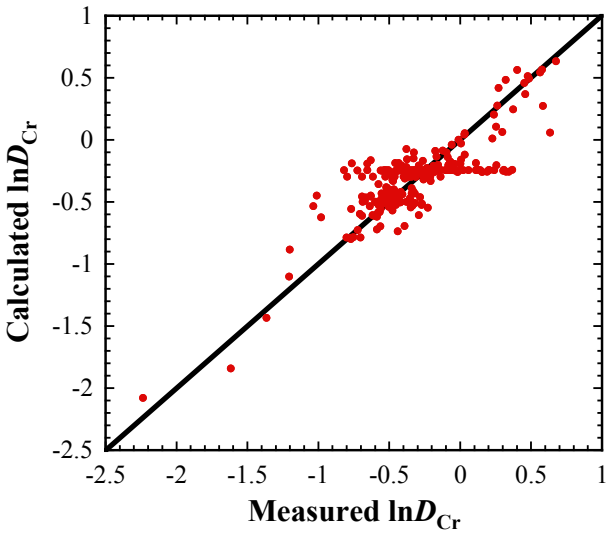

Figure 7. Fit of Cr partition coefficient data using equation (2) with parameters given in Equations (3a) to (3c). Literature Cr partition data are from EarthChem (Nielsen and Ustunisik 2019), Beattie (1994), Canil (1998, 1999), Hanson and Jones (1998), Righter et al. (2004), Mallmann and O'Neill (2009, 2013), Tuff and O'Neill (2010), Fellows and Canil (2012), Davis et al. (2013), Bell et al. (2014), Fonseca et al. (2014), Liu et al. (2014), and Leizke et al. (2016). Fifteen data points are excluded, including 7 points in Mallmann and O'Neill (2009), 3 in Fonseca et al. (2014), 3 in Leitzke et al. (2016), and 2 points in Liu et al. (2014).

Vanadium partitioning has been evaluated systematically in numerous studies and has been found to be insensitive to temperature or composition but to increase strongly with decreasing

435 fO_2 (e.g. Canil 1997; Mallmann and O'Neill 2009, 2013; Papike et al. 2013). Therefore,
436 partitioning of V has been used as an important redox indicator (e.g. Canil and Fedortchouk 2001;
437 Shearer et al. 2006; Wood et al. 2008; Mallmann and O'Neill 2013). The V partition coefficient
438 data for lunar samples range from 0.17 to 0.74, with an average of ~0.43, and are systematically
439 higher than the values of 0.003 to 0.21 reported for terrestrial basalts (Table 3). This result is
440 expected because lunar basalts are much more reduced than terrestrial basalts. For example,
441 XANES measurements of lunar samples show that V in lunar basalts is predominantly in the
442 form of V^{3+}, with up to 20% of V^{2+} (Sutton and Newville 2005; Karner et al. 2006). The
443 dominant valence state in terrestrial basalts, however, is V^{4+} (Papike et al. 2005), which explains
444 the difference in V partition coefficients between lunar and terrestrial samples. The observed
445 variation of V partition coefficient from 0.17 to 0.74 in lunar basalts can be explained by
446 variations of $\log fO_2$, from NNO – 3.17 to NNO – 5.86 (IW + 1.5 to IW – 1.2) according to the
447 relationship between D_V and $\log fO_2$ of Canil (1997), or from IW + 1.5 to IW – 1.8 using the
448 model of Mallmann and O'Neill (2009), which are roughly consistent with the estimated oxygen
449 fugacity for lunar basalts (IW-2 to IW, Sato et al. 1973; Wadhwa 2008). There may also be
450 significant dependence of V partition coefficient on melt composition, as recently modeled
451 empirically by Mallmann and O'Neill (2013). However, although the model by Mallmann and
452 O'Neill (2013) attempted to improve the model of Mallmann and O'Neill (2009) by
453 incorporating the compositional dependence of D_V, it fails to reproduce the measured D_V values
454 in this study by assuming a reasonable fO_2 for lunar basalts (from IW to IW-2): the predicted D_V

455 values would be too high by up to 1.5 orders of magnitude. This points to the limitations of
456 empirical modeling of the partition coefficient of V, which has multiple oxidation states. Due to
457 the difficulty in our modeling of Cr partition coefficient, and because there are more potential
458 oxidation states for V, we did not attempt to model V partition coefficient using a
459 thermodynamically-based formulation. Nonetheless, our data on V partitioning are as expected.
460

461 **4.2. Implications**

462 The olivine-melt partition coefficients for lunar mare basalts obtained in this study may be
463 applied to investigate the effect of olivine fractionation during lunar basaltic magma evolution
464 and shallow-level (low pressure) lunar magma ocean evolution. In addition, our data for
465 olivine-melt partitioning can be combined with partition data between other mantle minerals and
466 melt to quantify trace element behavior during lunar mantle partial melting and trace element
467 concentration in primary mare basalts and the lunar mantle.

468 Data for most elements in this study for lunar olivine-melt partitioning are similar to those
469 for terrestrial basalts. Hence, no reconsideration is needed for relevant modeling for those
470 elements. However, Li, V, and Cr partition coefficients between olivine and melt in lunar basalts
471 are significantly different from those in terrestrial basalts. There are several consequences of this.

472 As shown in Figure 6a, Li becomes a compatible element in olivine when the Fa# in olivine
473 is greater than 0.25, which roughly corresponds with a low Mg# $\leq$ 0.47 in the melt using a K_D
474 value of 0.3. That is, in evolved basalt, Li is compatible in olivine. However, because the Li

475 partition coefficient in pyroxenes is smaller than that in olivine (Ottolini et al. 2009), the effect of
476 the increased compatibility of Li in olivine in evolved basalt does not appear to result in a clear
477 shift in Li behavior when lunar basalts and terrestrial basalts are compared. Hence, it does not
478 seem that the slightly different Li partition coefficient results in significantly different behavior
479 between lunar basalts and terrestrial basalts.

480 The Cr partition coefficient between olivine and melt is smaller in lunar basalts than in
481 terrestrial basalts. Combined with the observation that Cr partition coefficient between
482 clinopyroxene and melt and between orthopyroxene and melt decreases with decreasing fO_2
483 (Canil, 1999; Mallmann and O'Neill, 2009), Cr is an incompatible element during lunar mantle
484 partial melting and early basalt evolution, which is opposite to it being strongly compatible
485 during terrestrial mantle partial melting and basalt evolution. Therefore, Cr concentration in
486 mantle-derived basalts is expected to be high, and to become higher in evolved melts before
487 oxide minerals crystallize. That is, the higher Cr concentration in lunar olivine than terrestrial
488 olivine (e.g., Steele and Smith, 1975) is not due to larger Cr partition coefficient, but to higher Cr
489 concentration in the melt (Schreiber and Haskin, 1976).

490 Figure 8 displays Cr versus MgO and Cr versus FeO in terrestrial and lunar basalts. MgO is
491 a compatible oxide and lower MgO concentration typically means more evolved basalts. Cr
492 concentrations in lunar basalts are much higher than in terrestrial MORB and OIB, as expected
493 from its incompatibility in the lunar mantle and its compatibility in the terrestrial mantle.
494 Furthermore, in terrestrial MORB and OIB, Cr shows a relatively simple positive (roughly

linearly) correlation with MgO, indicating that Cr is a compatible element similar to MgO during terrestrial basalt evolution. On the other hand, the Cr versus MgO trend in lunar basalts is more complicated: Cr concentration increases with decreasing MgO from 25 to approximately 11 wt%, and then decreases with further decreasing MgO. Hence, Cr is incompatible when MgO concentration is above 11 wt% (primitive basalt), but becomes compatible when MgO concentration is below 11 wt%. The trend of first increasing and then decreasing Cr concentration as MgO decreases in lunar basalts is similar to the FeO versus MgO trend in terrestrial basalts (Grove and Baker 1984) and might be controlled by the crystallization of chromite and/or other oxide minerals. In Cr versus FeO (Figure 8b), Cr is crudely positively correlated with FeO in lunar basalts (Seifert and Ringwood 1988) with Cr being more incompatible than FeO, indicating that Cr and Fe are both incompatible during mafic silicate mineral fractionation and compatible in Fe-Ti oxides. On the other hand, in terrestrial basalts, Cr concentration has a maximum at approximately 9 wt% FeO in MORB and 12 wt% FeO in OIB because starting from the maximum Cr concentration, tholeiitic FeO enrichment is accompanied by Cr depletion (Cr is compatible), and subsequent FeO depletion due to oxide crystallization is also accompanied by Cr depletion.

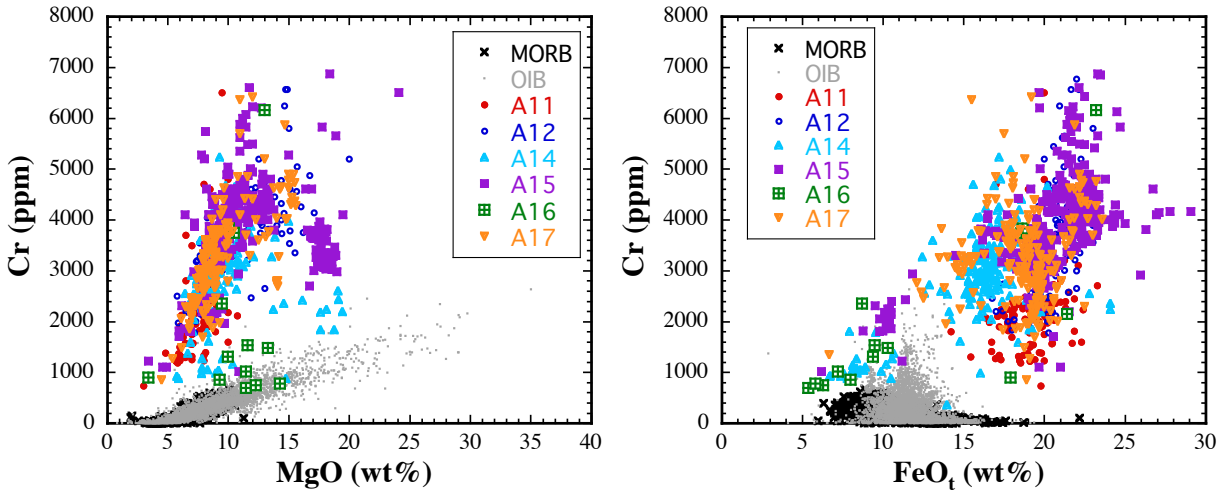

Figure 8. Cr concentration versus MgO and Cr versus FeO_t in lunar basalts and terrestrial MORB and OIB ($SiO_2 \leq 55$ wt%). Lunar basalt data are from Mare Basalt Database (https://www3.nd.edu/~cneal/lunar-l/), MORB data are from the compilation by Gale et al. (2013) and OIB data are from GeoRoc.

Vanadium partition coefficient between olivine and melt is higher in lunar settings than in terrestrial settings because of the more reduced lunar conditions. Combined with increasing V partition coefficients between other mafic minerals and melt as fO_2 decreases (Mallmann and O'Neill 2009), V is expected to be less incompatible during lunar basalt evolution than in terrestrial basalt evolution. Figure 9 confirms this expectation. In terrestrial basalts, V is highly incompatible in primitive basalts whereas Mg is compatible. Hence, V concentration increases steeply as MgO concentration decreases (Figure 9a, MORB and OIB trends). At lunar conditions, however, V is incompatible when MgO is greater than approximately 11 wt% (meaning that V concentration increases as MgO concentration decreases), but less so than in terrestrial basalts. At lower MgO, V in lunar basalts becomes compatible and decreases as MgO decreases. Vanadium concentration in lunar basalts when plotted against MgO also has a maximum at

approximately 10 to 12 wt% MgO, which is similar to Cr. The positive trends of V-FeO_t for both terrestrial and lunar samples but with a lower slope for lunar samples also indicate that V in terrestrial basalts is much more incompatible than in lunar basalts.

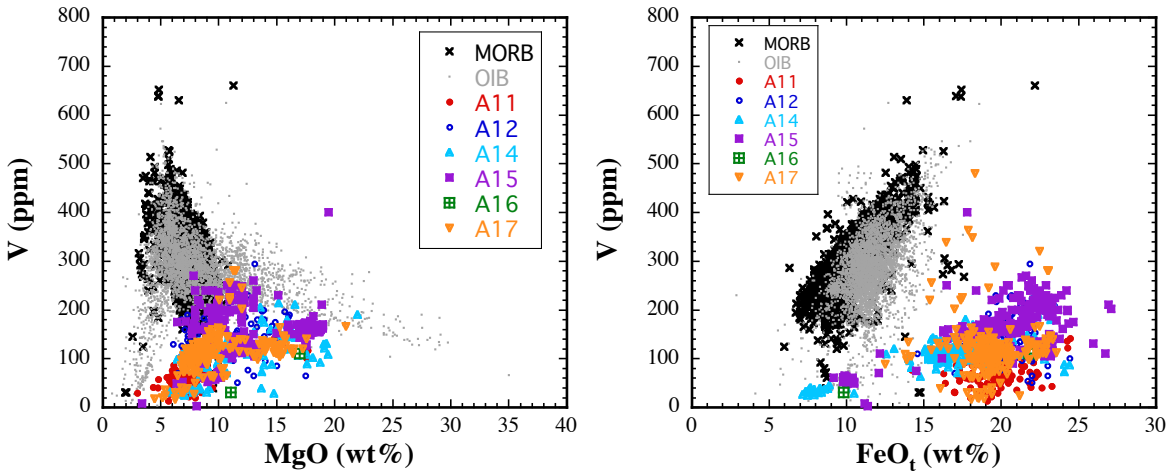

Figure 9. Vanadium concentration versus MgO and FeO in lunar and terrestrial basalts. Data sources are the same as Figure 8.

The partition coefficients of V and Cr between olivine and melt are similar in lunar basalts (0.17 to 0.74 for V versus 0.11 to 0.62 for Cr). However, in terrestrial basalts, the partition coefficient for V is much smaller than that of Cr. Hence, olivine fractionation would not significantly change the V/Cr ratio in the lunar magma ocean or lunar basalts, but V/Cr ratio in terrestrial basalts would increase significantly with olivine fractionation. The similarity of V and Cr partition coefficients between olivine and melt in lunar basalts apparently also applies to other mafic minerals in lunar settings, which leads to a nearly constant V/Cr ratio in lunar basalts (Seifert and Ringwood 1988). Figure 10 shows V versus Cr concentrations in lunar basalts and

545 terrestrial MORB and OIB, and indicates that V and Cr are positively correlated in lunar basalts
546 (Figure 10a) with nearly constant V/Cr ratio. Because some authors argue that the constancy of
547 an elemental ratio is best examined by using a log-log concentration plot (Sims and DePaolo,
548 1997; Hofmann et al. 2020), we do so in Figure 10b. A slope of 1 in the log-log plot means a
549 constant V/Cr ratio. In Figure 10b, even though there is much scatter (most of the very low V/Cr
550 ratios are from A11 samples, and most of the high V/Cr ratios are from A17 samples), the slope
551 from simple linear fitting of log(V) versus log(Cr) is 0.956±0.037 (1σ error), which is
552 approximately 1. After removing the outliers (outside 3σ), the average V/Cr slope in lunar
553 basalts is 0.039±0.011, which is in excellent agreement with the ratio of 0.038 obtained by
554 Seifert and Ringwood (1988). The V/Cr ratio in lunar basalts is not much different from the ratio
555 in the bulk silicate Earth (0.031, McDonough and Sun 1995). The depletion of Cr (50%
556 condensation temperature is 1296 K by Lodders 2003, 1291 K by Wood et al. 2019) in the Moon
557 relative to V (condensation temperature is 1429 K by Lodders 2003, 1370 K by Wood et al. 2019)
558 is ssmall, about 20% based on the ratios, which is within but the errors of the V/Cr ratios.
559 Because the data in Figure 10 reflect the involvement of not only olivine but also other
560 minerals, Figure 10 shows that V and Cr have similar degrees of incompatibility not only in
561 olivine as shown in this study, but also in other minerals in lunar basalts. Because element pairs
562 with nearly constant ratios are often used to estimate the mantle composition (e.g., McDonough
563 and Sun 1995; Salters and Stracke 2003; Hofmann et al. 2020) as well as particular processes
564 that might affect a given ratio (e.g., Cooper et al. 2012), the similar degree of incompatibility for

V and Cr provides a useful tool for examining lunar basalt evolution, as well as the lunar mantle composition.

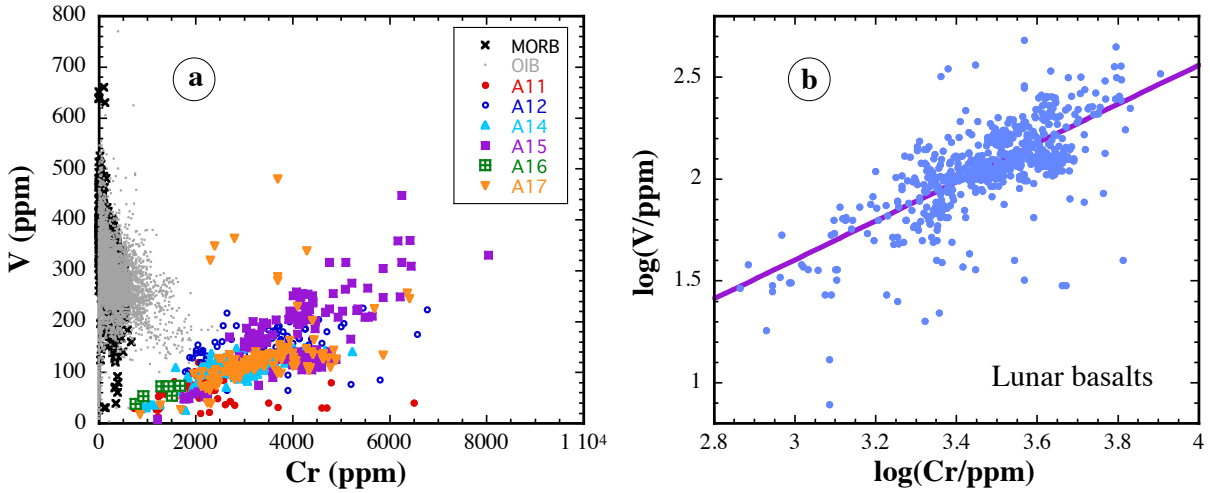

Figure 10. Vanadium concentration versus Cr concentration in lunar and terrestrial basalts. Data sources are the same as Figure 8.

To conclude, partition coefficients between olivine and melt in lunar basalts are measured for 21 elements. Most of our new data are in good agreement with those in terrestrial basalts despite the large differences in basalt composition and oxygen fugacity, except for the partition coefficients of Li, V and Cr. The slightly higher Li partition coefficient between olivine and melt in lunar basalts than terrestrial basalts is largely due to the higher Fa# in olivine in typical lunar basalts, and does not seem to lead to clear and consistent consequences in Li behavior during lunar basalt evolution. The higher V partition coefficients in lunar basalts can be readily explained by the lower oxidation state of lunar basalts compared to terrestrial basalts. On the other hand, the smaller partition coefficients of Cr in lunar basalts than in terrestrial basalts seem

to be due to compositional effects. Chromium behaves as an incompatible element during crystal fractionation of lunar basalt when MgO is ≥ 11 wt%, which is opposite to its compatibility during terrestrial basalt evolution. Vanadium is less incompatible during lunar basalt evolution than terrestrial basalt evolution. In addition, V and Cr have similar partition coefficients between mafic minerals and basalt in the Moon, confirming the results by Seifert and Ringwood (1988). Our new partition data can also explain: 1) the much higher Cr concentration in high-FeO lunar basalts than in terrestrial basalts, 2) the much lower V concentration in evolved lunar basalts than in evolved terrestrial basalts, and 3) the roughly constant V/Cr ratio of approximately 0.039 in lunar basalts (Seifert and Ringwood 1988). The partition coefficients determined in this study can be applied to model lunar magma evolution, to infer melt composition from olivine composition, and to model partial melting of the lunar mantle.

Acknowledgements:

We thank Dante Danil and an anonymous reviewer for their constructive reviews, which significantly improved this paper. This work was supported by NASA grant NNX15AH37G and 80NSSC19K0782,and NSF grant EAR-2020603. We thank NASA CAPTEM for providing the lunar samples, K.P. Jochum for providing the MPI-DING glass standards, J.C. Barrette for assistance in LA-ICP-MS analyses, and Yunbin Guan for assistance in SIMS analyses.

References:

Agee, C.B., and Walker, D. (1990) Aluminum partitioning between olivine and ultrabasic silicate liquid to 6 GPa. Contributions to Mineralogy and Petrology, 105, 243–254.
Beattie, P. (1994) Systematics and energetics of trace-element partitioning between olivine and silicate melts: Implications for the nature of mineral/melt partitioning. Chemical Geology, 117, 57–71.
Bell, A.S., Burger, P.V., Le, L., Shearer, C.K., Papike, J.J., Sutton, S.R., Newville, M., and Jones, J. (2014) XANES measurements of Cr valence in olivine and their applications to planetary basalts. American Mineralogist, 99, 1404–1412.
Berry, A.J., O'Neill, H.S.C., Scott, D.R., Foran, G.J., and Shelley, J.M.G. (2006) The effect of composition on Cr^{2+}/Cr^{3+} in silicate melts. American Mineralogist, 91, 1901–1908.
Blundy, J., and Wood, B. (1994) Prediction of crystal–melt partition coefficients from elastic moduli. Nature, 372, 452–454.
Borisov, A., Lahaye, Y., and Palme, H. (2004) The effect of TiO_2 on Pd, Ni, and Fe solubilities in silicate melts. American Mineralogist, 89, 564–571.
Brenan, J.M., Neroda, E., Lundstrom, C.C., Shaw, H.F., Ryerson, F.J., and Phinney, D.L. (1998) Behavior of boron, beryllium, and lithium during melting and crystallization: Constraints from mineral-melt partitioning experiments. Geochimica et Cosmochimica Acta, 62, 2129-2141.
Bucholz, C.E., Gaetani, G.A., Behn, M.D., and Shimizu, N. (2013) Post-entrapment modification of volatiles and oxygen fugacity in olivine-hosted melt inclusions. Earth and Planetary Science Letters, 374, 145–155.
Canil, D. (1997) Vanadium partitioning and the oxidation state of Archaean komatiite magmas. Nature, 389, 842–845.
——— (2002) Vanadium in peridotites, mantle redox and tectonic environments: Archean to present. Earth and Planetary Science Letters, 195, 75–90.
Canil, D., and Fedortchouk, Y. (2001) Olivine-liquid partitioning of vanadium and other trace elements, with applications to modern and ancient picrites. The Canadian Mineralogist, 39, 319–330.
Charlier, B., Grove, T.L., Namur, O., and Holtz, F. (2018) Crystallization of the lunar magma ocean and the primordial mantle-crust differentiation of the Moon. Geochimica et Cosmochimica Acta, 234, 50–69.
Chen, Y., and Zhang, Y. (2008) Olivine dissolution in basaltic melt. Geochim. Cosmochim. Acta, 72, 4756-4777.
Chen, Y., and Zhang, Y. (2009) Clinopyroxene dissolution in basaltic melt. Geochim. Cosmochim. Acta, 73, 5730-5747.
Chen, Y., Provost, A., Schiano, P., and Cluzel, N. (2011) The rate of water loss from olivine-hosted melt inclusions. Contributions to Mineralogy and Petrology, 162, 625–636.
——— (2013) Magma ascent rate and initial water concentration inferred from diffusive water loss from olivine-hosted melt inclusions. Contributions to Mineralogy and Petrology, 165,

525–541.
Chen, Y., Zhang, Y., Liu, Y., Guan, Y., Eiler, J., and Stolper, E.M. (2015) Water, fluorine, and sulfur concentrations in the lunar mantle. Earth and Planetary Science Letters, 427, 37–46.
Cottrell, E., and Kelley, K.A. (2011) The oxidation state of Fe in MORB glasses and the oxygen fugacity of the upper mantle. Earth and Planetary Science Letters, 305, 270–282.
Dalou, C., Koga, K.T., Shimizu, N., Boulon, J., and Devidal, J.L. (2012) Experimental determination of F and Cl partitioning between lherzolite and basaltic melt. Contributions to Mineralogy and Petrology, 163, 591-609.
Donaldson, C.H., Usselman, T.M., Williams, R.J., and Lofgren, G.E. (1975) Experimental modeling of the cooling history of Apollo 12 olivine basalts. 6th Lunar Science Conference, 843–869.
Duke, J.M. (1976) Distribution of the Period Four Transition Elements among Olivine, Calcic Clinopyroxene and Mafic Silicate Liquid: Experimental Results. Journal of Petrology, 17, 499–521.
Dunn, T., and Sen, C. (1994) Mineral/matrix partition coefficients for orthopyroxene, plagioclase, and olivine in basaltic to andesitic systems: A combined analytical and experimental study. Geochimica et Cosmochimica Acta, 58, 717–733.
Dygert, N., Liang, Y., and Hess, P. (2013) The importance of melt TiO_2 in affecting major and trace element partitioning between Fe–Ti oxides and lunar picritic glass melts. Geochimica et Cosmochimica Acta, 106, 134–151.
Elardo, S.M., Draper, D.S., and Shearer, C.K. (2011) Lunar Magma Ocean crystallization revisited: Bulk composition, early cumulate mineralogy, and the source regions of the highlands Mg-suite. Geochimica et Cosmochimica Acta, 75, 3024–3045.
Evans, T.M., C. O'Neill, H.St., and Tuff, J. (2008) The influence of melt composition on the partitioning of REEs, Y, Sc, Zr and Al between forsterite and melt in the system CMAS. Geochimica et Cosmochimica Acta, 72, 5708–5721.
Fonseca, R.O.C., Mallmann, G., Sprung, P., Sommer, J.E., Heuser, A., Speelmanns, I.M., and Blanchard, H. (2014) Redox controls on tungsten and uranium crystal/silicate melt partitioning and implications for the U/W and Th/W ratio of the lunar mantle. Earth and Planetary Science Letters, 404, 1–13.
Gaetani, G.A. and Grove, T.L. (1997) Partitioning of moderately siderophile elements among olivine, silicate melt, and sulfide melts: Constraints on core formation in the Earth and Mars. Geochimica et Cosmochimica Acta, 61, 1829–1846.
Gaetani, G.A., and Watson, E.B. (2000) Open system behavior of olivine-hosted melt inclusions. Earth and Planetary Science Letters, 183, 27–41.
——— (2002) Modeling the major-element evolution of olivine-hosted melt inclusions. Chemical Geology, 183, 25–41.
Gaetani, G.A., O'Leary, J.A., Shimizu, N., Bucholz, C.E., and Newville, M. (2012) Rapid reequilibration of H_2O and oxygen fugacity in olivine-hosted melt inclusions. Geology, 40,

915–918.
Gale, A., Dalton, C.A., Langmuir, C.H., Su, Y., and Schilling, J.-G. (2013) The mean composition of ocean ridge basalts. Geochemistry, Geophysics, Geosystems, 14, 489–518.
Grant, K.J., and Wood, B.J. (2010) Experimental study of the incorporation of Li, Sc, Al and other trace elements into olivine. Geochimica et Cosmochimica Acta, 74, 2412–2428.
Grove, T.L., and Baker, M.B. (1984) Phase equilibrium controls on the tholeiitic versus calc-alkaline differentiation trends. Journal of Geophysical Research, 89, 3253-3274.
Hanson, B., and Jones, J.H. (1998) The systematics of Cr^{3+} and Cr^{2+} partitioning between olivine and liquid in the presence of spinel. American Mineralogist, 83, 669–684.
Hart, S.R., and Davis, K.E. (1978) Nickel partitioning between olivine and silicate melt. Earth and Planetary Science Letters, 40, 203–219.
Hofmann, A.W., Class, C. and Goldstein, S.L. (2020) Size and composition of the residual and depleted mantle reservoir. Preprint. doi 10.1002/essoar.10501102.1.
Huebner, J.S., Lipin, B.R., and Wiggens, L.B. (1976) Partitioning of chromium between silicate crystals and melts. Proceedings of the 7th Lunar Science Conference, 1195–1220.
Jochum, K.P., Nohl, U., Herwig, K., Lammel, E., Stoll, B., and Hofmann, A.W. (2005) GeoRem: a new geochemical database for reference materials and isotopic standards. Geostand. Geoanal. Res., 29, 333-338.
Jochum, K.P., Stoll, B., Herwig, K., Willbold, M., Hofmann, A.W., Amini, M., Aarburg, S., Abouchami, W., Hellebrand, E., Mocek, B., Raczek, I., Stracke, A., Alard, O., Bouman, C., Becker, S., Ducking, M., Bratz, H., Klemd, R., de Briuin, D., Canil, D., Cornell, D., de Hoog, J., Dalpe, C., Danyushevsky, L., Eisenhauer, A., Gao, Y., Snow, J.E., Groschopf, N., Gunther, D., Latkoczy, C., Guillong, M., Hauri, E.H., Hofer, H.E., and etc. (2006) MPI-DING reference glasses for in situ microanalysis: new reference values for element concentrations and isotope ratios. Geochem. Geophys. Geosys., 7, Q02008, doi:10.1029/2005GC001060.
Jochum, K.P., Weis, U., Stoll, B., Kuzmin, D., Yang, Q., Raczek, I., Jacob, D.E., Stracke, A., Birbaum, K., Frick, D.A., Gunther, D., and Enzweiler, J. (2011) Determination of reference values for NIST SRM 610-617 glasses following ISO guidelines. Geostand. Geoanal. Res., 35, 397-429.
Jones, J.H. (1995) Trace element partitioning. Rock physics and phase relations, A handbook of physical constants, AGU Reference Shelf, 3, 73–104.
Karner, J.M., Sutton, S.R., Papike, J.J., Shearer, C.K., Jones, J.H., and Newville, M. (2006) Application of a new vanadium valence oxybarometer to basaltic glasses from the Earth, Moon, and Mars. American Mineralogist, 91, 270–277.
Kennedy, A.K., Lofgren, G.E., and Wasserburg, G.J. (1993) An experimental study of trace element partitioning between olivine, orthopyroxene and melt in chondrules: equilibrium values and kinetic effects. Earth and Planetary Science Letters, 115, 177–195.
Langmuir, C.H., Hanson, G.N., O'Hara, M.J., Bailey, D.K., Tarney, J., and Dunham, K.C. (1980) An evaluation of major element heterogeneity in the mantle sources of basalts. Philosophical

718 Transactions of the Royal Society of London. Series A, Mathematical and Physical Sciences,
719 297, 383–407.
720 Laubier, M., Grove, T.L., and Langmuir, C.H. (2014) Trace element mineral/melt partitioning
721 for basaltic and basaltic andesitic melts: An experimental and laser ICP-MS study with
722 application to the oxidation state of mantle source regions. Earth and Planetary Science
723 Letters, 392, 265–278.
724 Leeman, W.P., and Scheidegger, K.F. (1977) Olivine/liquid distribution coefficients and a test
725 for crystal-liquid equilibrium. Earth and Planetary Science Letters, 35, 247–257.
726 Leitzke, F.P., Fonseca, R.O.C., Michely, L.T., Sprung, P., Münker, C., Heuser, A., and
727 Blanchard, H. (2016) The effect of titanium on the partitioning behavior of high-field
728 strength elements between silicates, oxides and lunar basaltic melts with applications to the
729 origin of mare basalts. Chemical Geology, 440, 219–238.
730 Li, Y., and Audetat, A. (2012) Partitioning of V, Mn, Co, Ni, Cu, Zn, As, Mo, Ag, Sn, Sb, W, Au,
731 Pb, and Bi between sulfide phases and hydrous basanite melt at upper mantle conditions.
732 Earth and Planetary Science Letters, 355–356, 327–340.
733 Libourel, G. (1999) Systematics of calcium partitioning between olivine and silicate melt:
734 implications for melt structure and calcium content of magmatic olivines. Contributions to
735 Mineralogy and Petrology, 136, 63–80.
736 Lin, Y., Tronche, E.J., Steenstra, E.S., and van Westrenen, W. (2017a) Evidence for an early wet
737 Moon from experimental crystallization of the lunar magma ocean. Nature Geosci., 10,
738 14-18.
739 Lodders, K. (2003) Solar system abundances and condensation temperatures of the elements.
740 Astrophysical Journal, 591, 1220-1247.
741 Longhi, J. (1977) Magma oceanography 2: chemical evolution and crustal formation.
742 Proceedings 8th Lunar Science Conference, 601–621.
743 Longhi, J., Walker, D., and Hays, J.F. (1978) The distribution of Fe and Mg between olivine and
744 lunar basaltic liquids. Geochimica et Cosmochimica Acta, 42, 1545–1558.
745 Mallmann, G., and O'Neill, H.S.C. (2009) The Crystal/Melt Partitioning of V during Mantle
746 Melting as a Function of Oxygen Fugacity Compared with some other Elements (Al, P, Ca,
747 Sc, Ti, Cr, Fe, Ga, Y, Zr and Nb). Journal of Petrology, 50, 1765–1794.
748 Mallmann, G., and O'Neill, H.S.C. (2013) Calibration of an Empirical Thermometer and
749 Oxybarometer based on the Partitioning of Sc, Y and V between Olivine and Silicate Melt.
750 Journal of Petrology, 54, 933–949.
751 McDade, P., Blundy, J.D., and Wood, B.J. (2003) Trace element partitioning on the Tinaquillo
752 Lherzolite solidus at 1.5GPa. Physics of the Earth and Planetary Interiors, 139, 129–147.
753 Mikouchi, T., McKay, G., and Le, L. (1994) Cr, Mn, and Ca distributions for olivine in angritic
754 systems: Constraints on the origins of Cr-rich and Ca-poor core olivine in angrite LEW87051.
755 Lunar and Planetary Science, 25, 907–908.
756 Newton R. C., Anderson A. T. and Smith J. V. (1971) Accumulation of olivine in rock 12040

and other basaltic fragments in the light of analysis and syntheses. Proceedings 1st Lunar Science Conference , 575-582.
Ni, P., Zhang, Y., and Guan, Y. (2017) Volatile loss during homogenization of lunar melt inclusions. Earth and Planetary Science Letters, 478, 214–224.
Ni, P., Zhang, Y., Chen, S., and Gagnon, J. (2019) A melt inclusion study on volatile abundances in the lunar mantle. Geochimica et Cosmochimica Acta, 249, 17–41.
Nielsen, R.L., Gallahan, W.E., and Newberger, F. (1992) Experimentally determined mineral-melt partition coefficients for Sc, Y and REE for olivine, orthopyroxene, pigeonite, magnetite and ilmenite. Contributions to Mineralogy and Petrology, 110, 488–499.
Nielsen, R.L., and Ustunisik, G.K. (2019) EarthChem Data. Olivine/melt partition coefficient experiments, version 1.0. Interdisciplinary Earth Data Alliance (IEDA). https://doi.org/10.1594/IEDA/111285.
Nikogosian, I., and Sobolev, A. (1997) Ion-microprobe analysis of melt Inclusions in olivine: experience in estimating the olivine-melt partition coefficients of trace elements. Geochemistry International, 35, 119–126.
O'Neill, H.St.C., Berry, A.J., and Mallmann, G. (2018) The oxidation state of iron in Mid-Ocean Ridge Basaltic (MORB) glasses: Implications for their petrogenesis and oxygen fugacities. Earth and Planetary Science Letters, 504, 152–162.
Onuma, N., Higuchi, H., Wakita, H., and Nagasawa, H. (1968) Trace element partitioning between two pyroxenes and the host lava. Earth and Planetary Science Letters, 5, 47–51.
Ottolini, L., Laporte, D., Raffone, N., Devidal, J.L., and Le Fevre, B. (2009) New experimental determination of Li and B partition coefficients during upper mantle partial melting. Contributions to Mineralogy and Petrology, 157, 313-325.
Papike, J.J., Karner, J.M., and Shearer, C.K. (2005) Comparative planetary mineralogy: Valence state partitioning of Cr, Fe, Ti, and V among crystallographic sites in olivine, pyroxene, and spinel from planetary basalts. American Mineralogist, 90, 277–290.
Papike, J.J., Burger, P.V., Bell, A.S., Le, L., Shearer, C.K., Sutton, S.R., Jones, J., and Newville, M. (2013) Developing vanadium valence state oxybarometers (spinel-melt, olivine-melt, spinel-olivine) and V/(Cr+Al) partitioning (spinel-melt) for martian olivine-phyric basalts. American Mineralogist, 98, 2193–2196.
Paster, T.P., Schauwecker, D.S., and Haskin, L.A. (1974) The behavior of some trace elements during solidification of the Skaergaard layered series. Geochimica et Cosmochimica Acta, 38, 1549–1577.
Pearce, N.J.G., Perkins, W.T., Westgate, J.A., Gorton, M.P., Jackson, S.E., Neal, C.R., and Chenery, S.P. (1997) A Compilation of New and Published Major and Trace Element Data for NIST SRM 610 and NIST SRM 612 Glass Reference Materials. Geostandards Newsletter, 21, 115–144.
Rapp, J.F., and Draper, D.S. (2018) Fractional crystallization of the lunar magma ocean: updating the dominant paradigm. Meteor. Planet. Sci., 53, 1432-1455.

796 Roeder, P.L., and Emslie, R.F. (1970) Olivine-liquid equilibrium. Contributions to Mineralogy
797 and Petrology, 29, 275–289.
798 Rollinson, H.R. (1993) Using geochemical data: evaluation, presentation, interpretation.
799 Longman Scientific & Technical; Copublished in the U.S. with J. Wiley & Sons, Harlow,
800 Essex, England; New York.
801 Salters, V.J., and Stracke, A. (2004) Composition of the depleted mantle. Geochemistry
802 Geophysics Geosystems, 5, Q05004.
803 Sato, M., Hickling, N.L., and McLane, J.E. (1973) Oxygen fugacity values of Apollo 12, 14, and
804 15 lunar samples and reduced state of lunar magmas. Proc. 4th Lunar Sci. Conf. (Suppl.
805 Geochim. Cosmochim. Acta), 1, 1061-1079.
806 Schreiber, H.D., and Haskin, L.A. (1976) Chromium in basalts: Experimental determination of
807 redox states and partitioning among synthetic silicate phases. Proceedings of Lunar Science
808 Conference, 7, 1221–1259.
809 Seifert, S., and Ringwood, A.. E. (1988) The lunar geochemistry of chromium and vanadium.
810 Earth, Moon and Planets, 40, 45–70.
811 Shannon, R.D. (1976) Revised effective ionic radii and systematic studies of interatomic
812 distances in halides and chalcogenides. Acta Crystallographica Section A: Crystal Physics,
813 Diffraction, Theoretical and General Crystallography, 32, 751–767.
814 Sharp, M., Righter, K., and Walker, R.J. (2015) Estimation of trace element concentrations in the
815 lunar magma ocean using mineral- and metal-silicate melt partition coefficients. Meteoritics
816 & Planetary Science, 50, 733–758.
817 Shearer, C.K., McKay, G., Papike, J.J., and Karner, J.M. (2006) Valence state partitioning of
818 vanadium between olivine-liquid: Estimates of the oxygen fugacity of Y980459 and
819 application to other olivine-phyric martian basalts. American Mineralogist, 91, 1657–1663.
820 Simon, S.B., and Sutton, S.R. (2017) Valence of Ti, V, and Cr in Apollo 14 aluminous basalts
821 14053 and 14072. Meteoritics & Planetary Science, 52, 2051–2066.
822 Snyder, G.A., Taylor, L.A., and Neal, C.R. (1992) A chemical model for generating the sources
823 of mare basalts: Combined equilibrium and fractional crystallization of the lunar
824 magmasphere. Geochimica et Cosmochimica Acta, 56, 3809–3823.
825 Spandler, C., and O'Neill, H.S.C. (2010) Diffusion and partition coefficients of minor and trace
826 elements in San Carlos olivine at 1,300°C with some geochemical implications.
827 Contributions to Mineralogy and Petrology, 159, 791–818.
828 Solomon, S.C. and Longhi, J. (1977) Magma oceanography: 1. thermal evolution. Proceedings of
829 Lunar Science Conference, 8, 583-599.
830 Stead, C.V., Tomlinson, E.L., Kamber, B.S., Babechuk, M.G., and McKenna, C.A. (2017) Rare
831 Earth Element Determination in Olivine by Laser Ablation-Quadrupole-ICP-MS: An
832 Analytical Strategy and Applications. Geostandards and Geoanalytical Research, 41, 197–
833 212.
834 Steele, I.M., and Smith, J.V. (1975) Minor elements in lunar olivine as a petrologic indicator.

835 Proceedings of Lunar Science Conference, 6, 451-467.
836 Sun, C., and Liang, Y. (2012) Distribution of REE between clinopyroxene and basaltic melt
837 along a mantle adiabat: effects of major element composition, water, and temperature.
838 Contributions to Mineralogy and Petrology, 163, 807–823.
839 ——— (2013) The importance of crystal chemistry on REE partitioning between mantle
840 minerals (garnet, clinopyroxene, orthopyroxene, and olivine) and basaltic melts. Chemical
841 Geology, 358, 23–36.
842 Sutton, S.R., Jones, K.W., Gordon, B., Rivers, M.L., Bajt, S., and Smith, J.V. (1993) Reduced
843 chromium in olivine grains from lunar basalt 15555: X-ray Absorption Near Edge Structure
844 (XANES). Geochimica et Cosmochimica Acta, 57, 461–468.
845 Sutton, S.R., Karner, J., Papike, J., Delaney, J.S., Shearer, C., Newville, M., Eng, P., Rivers, M.,
846 and Dyar, M.D. (2005) Vanadium K edge XANES of synthetic and natural basaltic glasses
847 and application to microscale oxygen barometry. Geochimica et Cosmochimica Acta, 69,
848 2333–2348.
849 Suzuki, T., and Akaogi, M. (1995) Element partitioning between olivine and silicate melt under
850 high pressure. Physics and Chemistry of Minerals, 22, 411–418.
851 Taura, H., Yurimoto, H., Kurita, K., and Sueno, S. (1998) Pressure dependence on partition
852 coefficients for trace elements between olivine and the coexisting melts. Physics and
853 Chemistry of Minerals, 25, 469–484.
854 Taylor, S.R. and Jakes, P. (1974) The geochemical evolution of the moon. Proceedings 5th Lunar
855 Science Conference, 1287-1305.
856 Thomas, J.B., Bodnar, R.J., Shimizu, N., and Sinha, A.K. (2002) Determination of zircon/melt
857 trace element partition coefficients from SIMS analysis of melt inclusions in zircon.
858 Geochimica et Cosmochimica Acta, 66, 2887–2901.
859 Toplis, M.J., and Carroll, M.R. (1995) An Experimental Study of the Influence of Oxygen
860 Fugacity on Fe-Ti Oxide Stability, Phase Relations, and Mineral—Melt Equilibria in
861 Ferro-Basaltic Systems. Journal of Petrology, 36, 1137–1170.
862 Usselman, T.M., Lofgren, G.E., Donaldson, C.H., and Williams, R.J. (1975) Experimentally
863 reproduced textures and mineral chemistries of high-titanium mare basalts. Proceedings of
864 Lunar Science Conference 6, 997-1020.
865 Wadhwa, M. (2008) Redox Conditions on Small Bodies, the Moon and Mars. Reviews in
866 Mineralogy and Geochemistry, 68, 493–510.
867 Walker, D., kirkpatrick, R.J., Longhi, J., and Hays, J.F. (1976) Crystallization history of lunar
868 picritic basalt sample 12002: Phase-equilibria and cooling-rate studies. Geological Society of
869 America Bulletin, 87, 646-656.
870 Watson, E.B. (1979) Calcium content of forsterite coexisting with silicate liquid in the system
871 Na_2O-CaO-MgO-Al_2O_3-SiO_2. American Mineralogist, 64, 824–829.
872 Wood, B.J., Smythe, D.J., and Harrison, T. (2019) The condensation temperatures of the
873 elements: a reappraisal. American Mineralogist, 104, 844-856.

874 Wood, B.J., Wade, J., and Kilburn, M.R. (2008) Core formation and the oxidation state of the
875 Earth: Additional constraints from Nb, V and Cr partitioning. Geochimica et Cosmochimica
876 Acta, 72, 1415–1426.
877 Wood, J.A., Dickey, J.S., Marvin, U.B., and Powell, B.N. (1970) Lunar anorthosites and a
878 geophysical model of the moon. Proceedings Apollo 11 Lunar Science Conference, 965–988.
879 Xirouchakis, D., Hirschmann, M.M., and Simpson, J.A. (2001) The effect of titanium on the
880 silica content and on mineral-liquid partitioning of mantle-equilibrated melts. Geochimica et
881 Cosmochimica Acta, 65, 2201–2217.
882 York, D. (1968) Least squares fitting of a straight line with correlated errors. Earth and Planetary
883 Science Letters, 5, 320–324.
884 Zajacz, Z., and Halter, W. (2007) LA-ICPMS analyses of silicate melt inclusions in
885 co-precipitated minerals: Quantification, data analysis and mineral/melt partitioning.
886 Geochimica et Cosmochimica Acta, 71, 1021–1040.
887 Zanetti, A., Tiepolo, M., Oberti, R., and Vannucci, R. (2004) Trace-element partitioning in
888 olivine: modelling of a complete data set from a synthetic hydrous basanite melt. Lithos, 75,
889 39–54.
890 Zhang, Y., Ni, H., and Chen, Y. (2010) Diffusion data in silicate melts. Reviews in Mineralogy
891 and Geochemistry, 72, 311-408.
892
893